CHEMISTRY OF MATERIALS

pubs.acs.org/cm

Article

Electron-Enhanced Atomic Layer Deposition of Titanium Nitride Films Using an Ammonia Reactive Background Gas

Zachary C. Sobell and Steven M. George*

Cite This: *Chem. Mater.* 2022, 34, 9624−9633

Read Online

ACCESS | Metrics & More | Article Recommendations

ABSTRACT: Electron-enhanced atomic layer deposition (EE-ALD) of titanium nitride (TiN) films was achieved using sequential exposures of tetrakis(dimethylamido)-titanium (TDMAT) and low energy electrons in the presence of a continuous NH_3 reactive background gas (RBG). Performing EE-ALD concurrently with a RBG is a new ALD film growth technique. The TiN EE-ALD was performed utilizing a hollow cathode plasma electron source (HC-PES). The HC-PES can deliver a high electron flux into background gases at pressures up to several mTorr. The TiN EE-ALD was conducted at temperatures of 30−70 °C using an electron acceleration voltage of 100 V and a NH_3 pressure of ∼1 mTorr. The incident electron flux promotes electron stimulated desorption (ESD) and facilitates rapid nucleation and low temperature film growth. The TiN EE-ALD film growth was achieved on a variety of substrates including a native oxide on silicon, a SiO_2 thermal oxide, and in situ silicon nitride films grown using electron-enhanced chemical vapor deposition (EE-CVD). Growth rates of 0.75 to 1.8 Å per cycle were measured using in situ four-wavelength ellipsometry for different TDMAT precursor exposures. Ex situ X-ray photoelectron spectroscopy (XPS) studies indicated that the TiN films were high purity and slightly nitrogen-rich. The in situ ellipsometry also measured low resistivities of ∼120 $\mu\Omega$ cm for the TiN films with thicknesses of ≥60 Å. These low resistivities were confirmed by ex situ four-point probe measurements and ex situ spectroscopic ellipsometry. X-ray diffraction investigations determined that the TiN EE-ALD films were crystalline. X-ray reflectivity studies also indicated that the thin TiN films had densities similar to bulk films. The high quality of the TiN EE-ALD films is attributed to the NH_3 RBG. Interaction between the low energy electrons and the NH_3 RBG is believed to form $\bullet NH_2$ and $\bullet H$ radical species that react with the surface during EE-ALD and improve film purity. The reactive $\bullet NH_2$ and $\bullet H$ species likely lead to nitridation and carbon removal from the films. RBGs greatly expand the possibilities for tuning film composition and properties during EE-ALD. In addition, TiN EE-ALD was accomplished on insulating substrates such as an SiO_2 thermal oxide. The TiN EE-ALD is believed to be possible on insulating substrates because the secondary electron yield for electron energies of ∼100 eV is greater than unity.

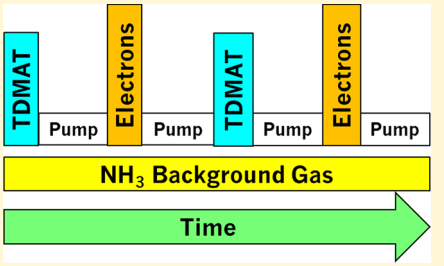

Downloaded via UNIV OF COLORADO BOULDER on November 24, 2022 at 03:43:25 (UTC).
See https://pubs.acs.org/sharingguidelines for options on how to legitimately share published articles.

1. INTRODUCTION

Low energy electrons can deposit films of semiconductors, metals, and dielectrics by electron-enhanced atomic layer deposition (EE-ALD). EE-ALD has been previously used to deposit GaN, Si, BN, and Co films in a high vacuum environment.[1−5] EE-ALD employs sequential exposures of precursors and low energy electrons at ≤ 100−150 eV to deposit these thin films. During EE-ALD, the precursor molecule adsorbs on the substrate. Subsequent electron exposure leads to a loss of ligands from the adsorbed precursor through electron stimulated desorption (ESD). The desorbed ligands leave behind open sites that are then available for further precursor adsorption. Repeating the sequential precursor doses and electron exposures yields EE-ALD growth.

The deposition of Si from disilane (Si_2H_6) can be considered a model system for EE-ALD.[4] Silicon was deposited using sequential surface reactions with Si_2H_6 and low energy electrons as the reactants.[4] The proposed mechanism was dissociative adsorption of Si_2H_6 on the surface and then the removal of hydrogen by ESD using low energy electrons. The removal of hydrogen from the surface leaves behind dangling bonds on the silicon surface. These dangling bonds are then available for subsequent Si_2H_6 adsorption. Silicon growth rates were determined to be 0.3 Å/cycle at room temperature and an electron energy of 100 eV. Calculations showed that this growth rate agrees well with the predicted growth rate based on dissociatively adsorbed Si_2H_6 on the dangling bonds of a Si surface.[4]

EE-ALD is a non-thermal process and can deposit materials at low temperatures <100 °C. The directional electron flux also leads to topographically selective deposition.[1] Surfaces that are normal to the electron flux receive a larger electron exposure

Received: July 31, 2022
Revised: September 26, 2022
Published: October 20, 2022

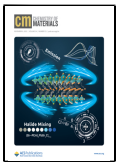

ACS Publications

© 2022 American Chemical Society

than surfaces parallel to the electron flux. This difference yields deposition primarily on surfaces normal to the direction of electron travel. In addition, large electron exposures lead to saturation of the ESD process by desorbing all the surface species. This desorption in the saturation limit produces a very conformal coverage of the deposited film. EE-ALD also has been shown to nucleate rapidly on a variety of surfaces.[1−5] Rapid nucleation should produce continuous films that may be important for ultrathin diffusion barriers and liners.

Titanium nitride (TiN) films have many applications. For example, TiN acts as a barrier to Cu diffusion.[6−8] Without a diffusion barrier, Cu readily diffuses into Si and SiO_2.[9,10] Ultrathin TiN diffusion barriers in small vias and trenches are important to maximize the amount of space that can be occupied by the Cu conducting line.[11,12] Rapid nucleation of TiN is critical to produce ultrathin continuous TiN films. In contrast, long nucleation times lead to thicker and rougher films prior to obtaining continuous films. TiN films also act as effective barriers to protect Ti and Si from chemical attack by WF_6 during W plug formation.[13] In addition, thin TiN films are used in the metal gate stack for CMOS.[14]

Previous TiN ALD films have required high deposition temperatures or have suffered from high porosity, low purity, and high resistivity.[6,15−21] Plasma-enhanced TiN deposition processes can result in more desirable film properties, but risk substrate damage from the high energy ions.[22,23] TiN deposition processes with $TiCl_4$ and NH_3 have additional drawbacks including the generation of corrosive HCl. Thermal TiN ALD with tetrakis(dimethylamido)titanium (TDMAT) and NH_3 has been shown to have high porosity and large C impurities.[15] The high porosity allows for facile oxidation.

In this investigation, TiN EE-ALD was performed using sequential exposures of TDMAT and low energy electrons in the presence of a continuous NH_3 reactive background gas (RBG) at a pressure of ∼1 mTorr. An illustration of this processing sequence is shown in Figure 1. The electrons can induce ESD of surface species to create reactive surface sites. The electrons can also dissociate NH_3 in the gas phase. The dissociation products of NH_3 help nitridate and purify the TiN film. A similar strategy has been employed in the field of focused electron beam-induced deposition (FEBID). High electron energies of ∼1 keV during FEBID lead to nearly complete dissociation of the gas precursors and high impurity levels in the FEBID films. Some FEBID studies have reported using a background gas, such as H_2O, O_2, or NH_3, during FEBID to attempt to reduce the impurity concentrations.[24−26] The use of an RBG in this study illustrates how an RBG also improves film purity during EE-ALD.

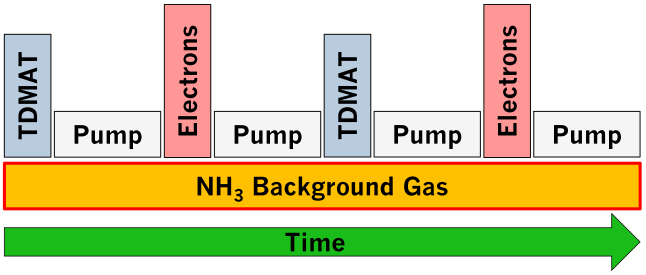

Figure 1. TiN EE-ALD process using sequential TDMAT and electron exposures with continuous NH_3 RBG.

2. EXPERIMENTAL SECTION

The TiN EE-ALD films were grown in a vacuum apparatus that has been described previously.[1−5] The main vacuum chamber is pumped by a turbomolecular pump. This turbomolecular pump has a pumping speed of 245 L/s for Ar (HiPace 300 P, Pfeiffer Vacuum Technology AG). This turbomolecular pump is also backed by a smaller turbomolecular pump operating at a pumping speed of 67 L/s for Ar (HiPace 80, Pfeiffer Vacuum Technology AG). This smaller turbomolecular pump is backed by a rotary vane pump (Pascal 2010 SD 10 m^3/h, Pfeiffer Vacuum Technology AG). Additionally, the main vacuum chamber can be pumped by an ion pump (TiTan 100 L Variable Element, 100 L/s, Gamma Vacuum). A valve can separate this ion pump from the main chamber. The main vacuum chamber had a base pressure of 2×10^{-9} Torr using both the ion and turbomolecular pumps.

This chamber was equipped with a load lock that allowed samples to be introduced without breaking vacuum. The main chamber also contained an in situ ellipsometer (Film Sense 1) and mass spectrometer (PrismaPlus QMG 220, Pfeiffer Vacuum). The chamber was also equipped with a cold cathode gauge (MKS) to measure pressure. In addition, a picoammeter (Keithley) was attached to the sample stage to measure the incident electron current from the electron source.

The electron source was a hollow cathode plasma electron source (HC-PES) that has been described in detail earlier.[1] An argon (Airgas, 99.999%) plasma was sparked in the hollow cathode body. Low energy electrons were extracted with a biased grid. The electrons exited the HC through an aperture. Argon gas also leaked through this aperture and produced a pressure of ∼1 mTorr in the reactor. All the work in this study used an applied voltage of 100 V to the biased grid. This applied voltage accelerated the electrons leaving the aperture. The electrons were separated from any sputtered material from the hollow cathode plasma using electron optics.[1] An analysis chamber containing an in vacuo Auger electron spectroscopy (AES) spectrometer (RBD, microCMA) was also attached to the main chamber.

NH_3 (Matheson, 99.9992%) flowed into the chamber though a leak valve and was present continuously during the TiN EE-ALD. The NH_3 RBG pressure was ∼1 mTorr as measured by the cold cathode pressure gauge under constant pumping using the turbomolecular pump. The background gases in the chamber will cause electron scattering. The recommended total cross section for electron scattering in NH_3 is $\sigma = 8.57 \times 10^{-16}$ cm^2 for electron energies of 100 eV.[27] In addition, the background Ar pressure in the chamber resulting from leakage through the aperture on the hollow cathode was ∼1 mTorr. The total cross section is $\sigma \sim 8 \times 10^{-16}$ cm^2 for electron scattering in Ar for electron energies of 100 eV.[28]

The mean free path for electrons traveling through gas is $\lambda_e = 1/\rho\sigma$, where ρ is the gas number density and σ is the cross section for electron scattering by the gas. The gas number density is $\sigma = 3.2 \times 10^{13}$ molecules/cm^3 at room temperature at a pressure of 1 mTorr. Therefore, the electron mean free path is $\lambda_e = 18$ cm using $\sigma \sim 8 \times 10^{-16}$ cm^2 for the Ar and NH_3 total cross sections. Electron scattering by the Ar and NH_3 RBG does not seriously affect the electron transport over the 25 cm distance between the HC-PES and the sample.

The TiN EE-ALD was explored on several substrates including Si wafer coupons, SiO_2 thermal oxide wafer coupons, and in situ deposited silicon nitride on Si wafer coupons. The Si wafer coupons (Silicon Valley Microelectronics, boron-doped) contained a native oxide on the silicon surface. The SiO_2 thermal oxide wafer coupons had a SiO_2 thickness of 400 nm on a Si wafer. Prior to insertion into the vacuum apparatus, the coupons were washed sequentially in methanol, acetone, and DI water and then blown dry with ultra-high purity nitrogen. The coupons were then loaded into the load lock chamber following procedures that have been detailed earlier.[1]

The in situ deposited Si_3N_4 films were grown using pulsed electron-enhanced chemical vapor deposition (EE-CVD). For this Si_3N_4-pulsed EE-CVD, a NH_3 RBG was flowed through the chamber during

https://doi.org/10.1021/acs.chemmater.2c02341
Chem. Mater. 2022, 34, 9624−9633

electron beam irradiation of the sample. Throughout this continuous electron beam and NH_3 exposure, Si_2H_6 was pulsed into the chamber every 5 s. In situ ellipsometry measurements observed that the Si_3N_4 films nucleated on the first Si_2H_6 pulse and grew linearly versus number of Si_2H_6 exposures. The Si_3N_4-pulsed EE-CVD films were grown to a thickness of ~10 nm. The Si_3N_4-pulsed EE-CVD films had high purity as measured by in vacuo AES. The films displayed a nearly stoichiometric 3:4 Si/N ratio with C and O impurities <2 at. %. In addition, the Si_3N_4 pulsed EE-CVD films were smooth as measured by ex situ atomic force microscopy (AFM) with an RMS roughness of <2 Å.

The TiN EE-ALD growth was conducted using a pulse sequence consisting of the following: (1) TDMAT dose; (2) pumping; (3) electron beam exposure; and (4) pumping before the next TDMAT dose. The timing for this pulsing sequence can be characterized by (t_1, t_2, t_3, t_4). During this pulse sequence, the NH_3 RBG existed concurrently at a pressure of ~1 mTorr.

For deposition on the silicon native oxide and the SiO_2 thermal oxide, the TDMAT precursor was maintained at 0.3 Torr behind a micropulse valve. The valve was actuated for t_1 = 1 s. The valve opening led to a transient pressure in the main chamber of 4×10^{-7} Torr as measured by the cold cathode gauge in an empty reactor. The pressure at the sample was higher because the micropulse valve was connected to a 1/4" diameter tube that led to the sample and ended ~5 cm from the sample. For deposition on the in situ deposited Si_3N_4, the valve was actuated for 2 s. The TDMAT pressure was 0.2 Torr behind the micropulse valve. These conditions yielded a transient pressure of 6×10^{-7} Torr in an empty reactor.

Pumping was then continued for t_2 = 2 s after the TDMAT exposure. Subsequently, the electron exposure was performed with a grid bias of 100 V for t_3 = 20 s, with an electron current measured at the sample stage of ~25 mA. The next TDMAT adsorption was then conducted after continued pumping for t_4 = 1 s after the electron exposure. The timing for this pulsing sequence was (1, 2, 20, 1). The sum of these steps produced a reaction cycle time of ~24 s. Note that the turbomolecular pump was pumping on the main vacuum chamber and the NH_3 RBG was present during the entire pulse sequence.

In situ ellipsometry measurements were collected every second throughout the deposition. The in situ ellipsometer used four wavelengths of light. The precision of the in situ ellipsometry measurements of film thickness was within ±0.03 Å. The in situ ellipsometer used a Drude−Lorentz model to model the TiN films. The software (Film Sense) was able to extrapolate resistivity from the model. Ex situ spectroscopic ellipsometry (Model M-2000, J.A. Woollam Co., Inc.) was also performed to measure the film thickness of some samples after removing them from the reactor. The data were fit using a Drude−Lorentz model with a Drude oscillator[29] (119 μΩ cm resistivity, 0.952 fs scattering time) and one Lorentzian oscillator (center energy: 5.385 eV, amplitude: 6.519, broadening: 3.980 eV).

A four-point probe (Signatone, QP2-MB8) was used for ex situ resistivity measurements. The probe spacing was 1 mm. The geometric correction factor was chosen based on the ratio of the probe spacing to the diameter of the largest inset circle possible on the wafer coupon. A typical geometric correction factor was 0.92. AFM measurements were used to monitor film roughness. The ex situ AFM measurements were performed with an AFM instrument (Park NX10) using the non-contact mode. The scan rate was 0.3−0.8 Hz for a 1 μm × 1 μm area using a micro cantilever probe (Olympus, OMCL-AC160TS).

X-ray reflectivity (XRR) was used to determine film thickness and density. Grazing incidence X-ray diffraction (GI-XRD) determined the crystallinity of the films. Both GI-XRD and XRR scans were performed using a XRD instrument (Bede D1, Jordan Valley Semiconductors) with radiation from Cu Kα (λ = 1.540 Å). The X-ray tube filament voltage was 40 kV and the current was 35 mA. The incident angle used for GI-XRD was 0.3°. The XRR scan range was 300−6000 arcsec with a 5 arcsec step size. The XRR scans were analyzed using modeling software (REFS, Jordan Valley Semiconductors).

The film composition was determined using an X-ray photoelectron spectrometer (PHI 5600 XPS) using a monochromatic Al Kα source with an energy of 1486.6 eV. The pass energy was 58.7 eV, the step size was 0.25 eV, and the dwell time was 50 ms per step. An electron beam neutralizer was used during the XPS measurements. The Ar ion beam energy during depth profiling was 3 keV. The XPS data were collected using Auger Scan (RBD Instruments) software. The XPS data were analyzed employing CASA XPS (Casa Software Ltd.) software.

3. RESULTS AND DISCUSSION

3.1. Nucleation Regime for TiN EE-ALD. The TiN EE-ALD films grown in the presence of the NH_3 RBG nucleated rapidly on the Si native oxide, thermal SiO_2, and the in situ deposited Si_3N_4 EE-CVD films. Figure 2 displays the growth of a TiN EE-ALD film on an in situ deposited Si_3N_4 EE-CVD film. These in situ ellipsometry measurements were performed in real time during TiN EE-ALD. The timing sequence in seconds was (2, 2, 20, 1) with a NH_3 RBG at ~1 mTorr and a TDMAT pressure of 0.2 Torr behind the micropulse valve. The TDMAT exposures produced a pressure transient of 6×10^{-7} Torr in an empty reactor.

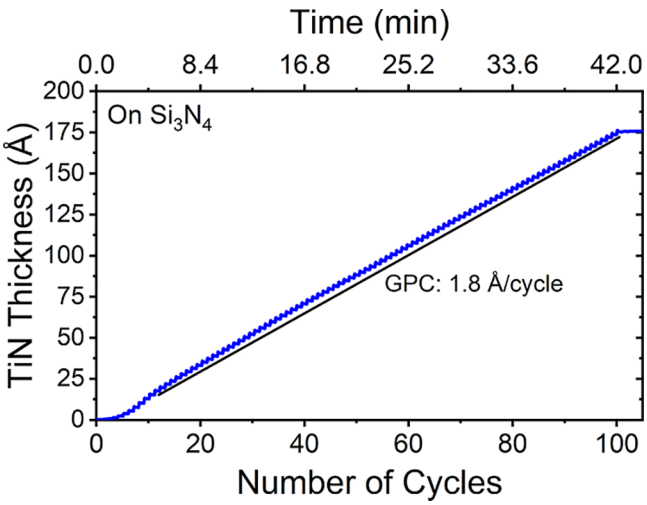

Figure 2. Nucleation and growth of TiN EE-ALD film thickness on Si_3N_4 vs number of EE-ALD cycles measured using in situ ellipsometry. Pulsing sequence in seconds was (2, 2, 20, 1) with a NH_3 background pressure of ~1 mTorr. GPC was 1.8 Å/cycle.

Figure 2 shows that the TiN EE-ALD film nucleates quickly and then grows with a growth per cycle (GPC) of 1.8 Å/cycle. Electrons were required for this TiN deposition. There was no TiN growth if the TDMAT exposures were performed without electrons from the HC-PES. An expansion of the first 10 EE-ALD cycles from the ellipsometric results in Figure 2 is given in Figure 3. The TiN EE-ALD reaches the GPC of 1.8 Å/cycle after only 5−6 cycles. The short nucleation delay of only 5−6 cycles allows for the deposition of continuous TiN films with thicknesses <1 nm.

Additional experiments determined that the TiN EE-ALD growth rates were dependent on the TDMAT precursor exposures. At higher TDMAT precursor exposures, the GPCs could reach >5 Å/cycle. These larger GPCs could be explained by larger TDMAT coverages adsorbed on the growing TiN surface after higher TDMAT exposures. Earlier experiments have confirmed that TDMAT adsorbs with a coverage-dependent sticking coefficient on TiN surfaces.[30] The

https://doi.org/10.1021/acs.chemmater.2c02341
Chem. Mater. 2022, 34, 9624−9633

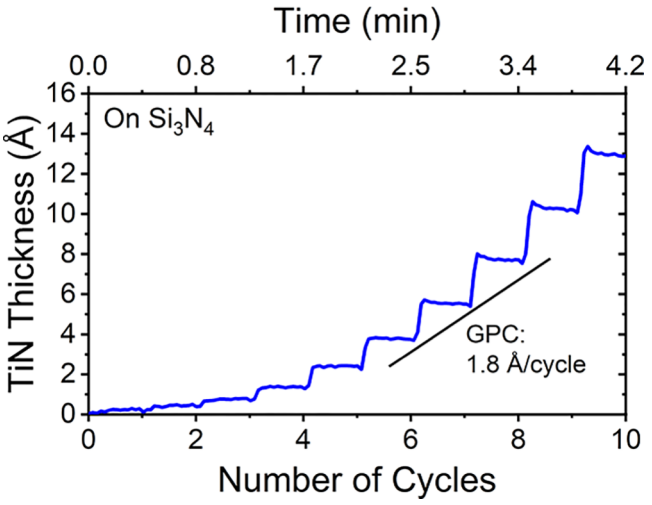

Figure 3. Expansion of the nucleation region in Figure 2 showing first 10 EE-ALD cycles. GPC of 1.8 Å/cycle was obtained after six EE-ALD cycles.

adsorbed TDMAT then desorbs with a coverage-dependent desorption rate.[30] The larger GPCs at higher TDMAT precursor exposures could affect the TiN film uniformity in high aspect ratio trench structures.

There also may be partial decomposition of TDMAT on electron-activated substrates through a mechanism such as autocatalytic deposition.[31−33] This mechanism could lead to the buildup of thick films with partially decomposed TDMAT precursors. To avoid these larger GPCs and higher carbon impurities in the TiN EE-ALD film, most of the results shown in this paper were obtained with shorter TDMAT precursor exposures of 1 s with TDMAT pressures of 0.3 Torr behind the micropulse valve. These TDMAT exposures produced a pressure transient of 4×10^{-7} Torr in an empty reactor.

The TiN EE-ALD films grown using the NH_3 RBG also nucleated rapidly on the Si native oxide. Figure 4 displays the TiN thickness versus number of EE-ALD cycles. The dosing sequence was (1−2−20−1) with a TDMAT pressure of 0.3 Torr behind the micropulse valve. Each data point represents a separate sample. The samples were removed from the reactor after a certain number of EE-ALD cycles for subsequent analysis. The TiN thickness increased linearly with the increase in number of cycles with a GPC of 0.76 Å/cycle. The GPC was lower because the TDMAT exposure was lower compared with the TDMAT exposures employed for Figures 2 and 3. A linear regression through the values for the TiN thickness versus number of EE-ALD cycles showed that the *x*-intercept was at 1 EE-ALD cycle. This *x*-intercept is interpreted as a nucleation delay of 1 EE-ALD cycle.

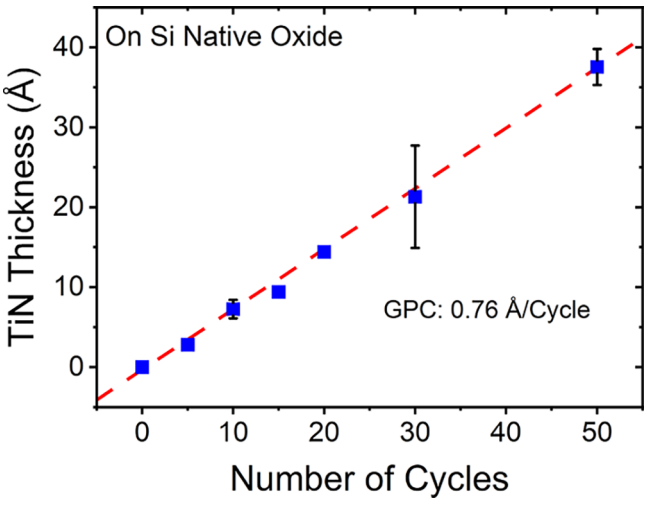

Figure 4. TiN EE-ALD film thickness on Si native oxide vs number of EE-ALD cycles measured using in situ ellipsometry. Pulsing sequence in seconds was (1, 2, 20, 1) with a NH_3 background pressure of ∼1 mTorr. GPC was 0.76 Å/cycle. Error bars are shown on points with more than one experiment.

The nucleation of TiN EE-ALD on Si native oxide was also explored using in vacuo AES after various numbers of EE-ALD cycles. These AES results are for the same set of samples as shown in Figure 4. After each TiN deposition, the main chamber was pumped down to ∼1×10^{-7} Torr. The sample was then transferred to the AES chamber, scanned to obtain the AES spectrum, and removed from the reactor for subsequent analysis. This process was repeated for 5, 10, 15, 20, 30, and 50 TiN EE-ALD cycles.

Figure 5 shows the results for the Ti/(Ti + Si) ratio of AES signals versus number of EE-ALD cycles. The Ti/(Ti + Si) ratio of AES signals increases linearly with the increase in number of cycles over the first 30 EE-ALD cycles. After ∼30 EE-ALD cycles, the Ti and Si AES signals reach limiting values because of the finite mean free path for the Auger electrons in the TiN film. As the TiN film progressively grows on the Si native oxide, the Ti AES signal reaches the limiting value for a bulk TiN film. The Si AES signal becomes completely attenuated by the overlying TiN film. The limiting value for the Ti/(Ti + Si) ratio at values slightly less than 100% can be explained by noise in the AES spectrum near the Si peak that leads to a finite apparent Si AES signal.

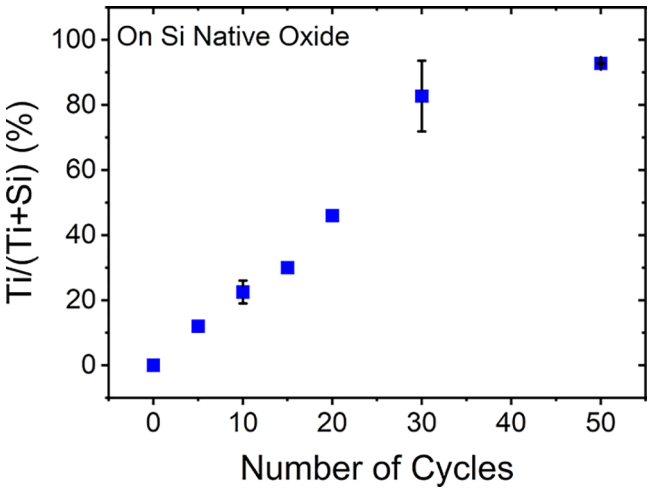

Figure 5. In vacuo AES measurement of ratio of AES signals Ti/(Ti + Si) (%) during TiN EE-ALD on Si native oxide vs number of EE-ALD cycles. Pulsing sequence in seconds was (1, 2, 20, 1) with NH_3 background pressure of ∼1 mTorr. Ti/(Ti + Si) (%) approaches 100% when TiN EE-ALD film blocks AES electrons from underlying Si substrate.

The roughness of the TiN EE-ALD films in the initial nucleation region on the Si native oxide was also studied by ex situ AFM measurements. These roughness results are for the same set of samples as shown in Figures 4 and 5. Figure 6

https://doi.org/10.1021/acs.chemmater.2c02341
Chem. Mater. 2022, 34, 9624−9633

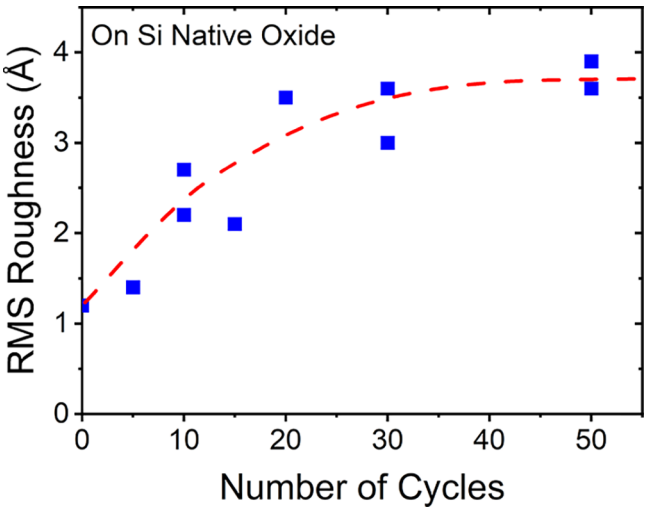

Figure 6. RMS roughness measured by AFM for the TiN EE-ALD film on Si native oxide vs number of EE-ALD cycles. Pulsing sequence in seconds was (1, 2, 20, 1) with a NH_3 background pressure of ~1 mTorr.

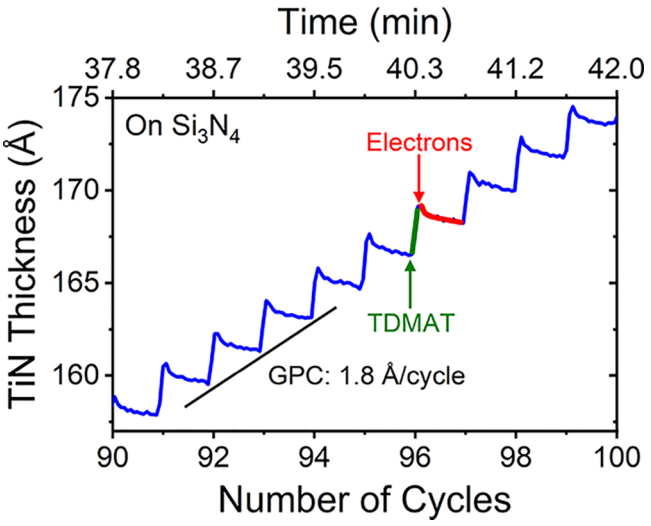

Figure 7. Expansion of the steady state region in Figure 2 showing TiN EE-ALD film thickness on Si_3N_4 vs number of EE-ALD cycles measured using in situ ellipsometry. Pulsing sequence in seconds was (2, 2, 20, 1) with a NH_3 background pressure of ~1 mTorr. GPC was 1.8 Å/cycle.

displays the RMS roughness values measured by the AFM versus number of EE-ALD cycles. The RMS roughness for a bare, cleaned Si coupon was ~4 Å. After a 5 min electron exposure with a NH_3 RBG at ~1 mTorr, the RMS roughness dropped to ~1 Å. This RMS roughness was used for the RMS roughness at 0 cycles of TiN EE-ALD in Figure 6. The RMS roughness then increases slowly by ~3 Å over 50 EE-ALD cycles. The resulting RMS surface roughness reaches a limiting value at ~4 Å.

The change in the surface roughness of the Si native oxide resulting from the initial 5 min electron exposure with NH_3 RBG motivated a study of the change in surface composition using in vacuo AES. One Si native oxide sample was loaded and irradiated with the electron beam and exposed to the NH_3 RBG at ~1 mTorr for 5 min with an electron sample current of 20 mA as a control. This control sample showed ~40 at. % N on the surface as measured by in vacuo AES. This N AES signal results from surface nitridation by $\bullet NH_2$ species from the electron beam interaction with the NH_3 RBG. In addition, the oxygen and carbon AES signals decreased by factors of 2.7 and 2.3, respectively, relative to initial Si native oxide samples that were not subjected to the electron exposures with NH_3 RBG. These experiments suggest that surface cleaning and smoothing result from the electron exposures with NH_3 RBG.

3.2. Steady State Growth for TiN EE-ALD. In situ ellipsometry was used to monitor the TiN EE-ALD in the steady state growth regime using sequential exposures of TDMAT and electrons with a NH_3 RBG in the chamber, as illustrated in Figure 1. Figure 7 shows the results for 10 cycles during 90−100 EE-ALD cycles on the in situ grown Si_3N_4 EE-CVD film. These 10 cycles were also displayed at a lower resolution in Figure 2. The dosing sequence was (2, 2, 20, 1) with a TDMAT pressure of 0.2 Torr behind the micropulse valve. The film thickness increases resulting from TDMAT adsorption during the TDMAT exposures. During the electron exposure, the TiN thickness decreases resulting from the ESD of surface species. The surface species are believed to be the dimethylamine ligands on the TDMAT adsorption products.

Initially the thickness decreases quickly during the electron exposure. Subsequently, there is a slow decrease of the thickness. This slow decrease may be the additional loss of dimethylamine ligands. An electron exposure of 20 s was chosen because shorter electron exposures led to higher C content in the films. The effect of the electron beam exposure time had a dramatic effect on the purity of the TiN film.

Figure 8 shows the in vacuo AES results for TiN EE-ALD films with and without the NH_3 RBG. The dosing sequence

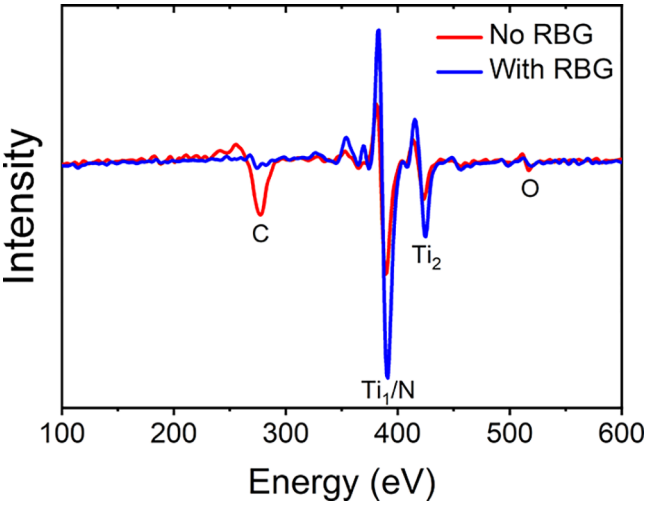

Figure 8. In vacuo AES showing AES signals for C, Ti, Ti/N, and O for TiN EE-ALD films grown on Si_3N_4. Pulsing sequence in seconds was (2, 2, 20, 1). TiN EE-ALD film grown with no RBG used 27 EE-ALD cycles. TiN EE-ALD film grown with NH_3 RBG utilized 50 EE-ALD cycles. C AES signal is much lower when NH_3 RBG was present at ~1 mTorr.

was (2, 2, 20, 1) with a TDMAT pressure of 0.2 Torr behind the micropulse valve. The TiN EE-ALD film grown with no NH_3 RBG used 27 EE-ALD cycles. The TiN EE-ALD film grown with the NH_3 RBG utilized 50 EE-ALD cycles. Without a NH_3 RBG, the in vacuo AES measured a C content in the as-deposited TiN film of ~60 at. %. In contrast, with the NH_3 RBG, the C content in the as-deposited TiN film was ~3 at. %.

https://doi.org/10.1021/acs.chemmater.2c02341
Chem. Mater. 2022, 34, 9624−9633

These results illustrate that the NH_3 RBG greatly enhances the purity of the TiN EE-ALD films.

In vacuo AES measurements also confirmed that the TiN EE-ALD films deposited with larger TDMAT precursor exposures contained more carbon. With the electron exposure held constant, the carbon content in the film increased for larger TDMAT precursor exposures. Carbon compositions of >30 at. % were observed when the GPC for TiN EE-ALD was 7 Å/cycle. These larger carbon contents were obtained with a TDMAT precursor exposure of 1 s with TDMAT pressure behind the micropulse valve of >0.6 Torr.

AES was able to quantify Si, O, and C using primary AES peaks, and Ti using a secondary AES peak. Unfortunately, the primary N AES peak overlapped with the primary Ti AES peak. There were no other useable N AES peaks. Consequently, ex situ XPS depth profiling was also used to quantify the TiN EE-ALD film composition. An XPS depth profile revealed very low impurities for a TiN EE-ALD film grown on Si native oxide with a dosing sequence of (1, 2, 20, 1) with a TDMAT pressure of 0.3 Torr behind the micropulse valve. The C and O contents were measured at 1.5 and 1.7 at. %, respectively. The Ti/N ratio was 1:1.17. The extra nitrogen may have been due to N stuffing at grain boundaries and vacancies. This N content in the grain boundaries may be beneficial for the diffusion barrier properties.[8,19]

GI-XRD was used to determine the crystallinity of the TiN EE-ALD films. Despite the low growth temperatures <70 °C, the TiN films display crystallinity. The GI-XRD results are shown in Figure 9 for a TiN EE-ALD film with a thickness of

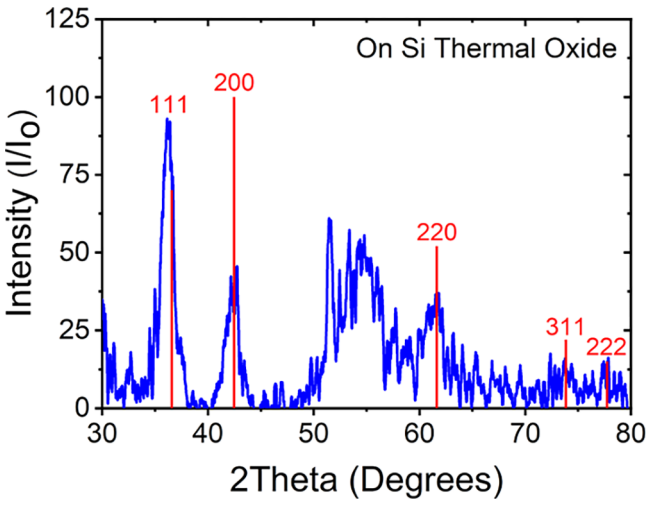

Figure 9. GI-XRD of TiN EE-ALD films grown on Si thermal oxide after 200 EE-ALD cycles. Pulsing sequence in seconds was (1, 2, 20, 1) with a NH_3 background pressure of ~1 mTorr. Miller indices of diffraction peaks for crystalline TiN are shown for comparison.

13.1 nm deposited on Si thermal oxide using 200 EE-ALD cycles. The dosing sequence was (1, 2, 20, 1) with a TDMAT pressure of 0.3 Torr behind the micropulse valve.

The (111) and (200) peaks of crystalline TiN match the diffraction peaks in Figure 9.[34] The (220), (311), and (222) peaks of crystalline TiN are also discernible above baseline. The Scherrer equation yields an average grain size of 8.9 nm from the (111) and (200) peaks. The broad peak at $2\theta \sim 55°$ is attributed to the (311) planes in crystalline silicon.[35]

X-ray reflectometry (XRR) was also used to measure the density of the TiN EE-ALD films. The average density of the films was 5.3 g/cm^3. This density is 98% of the theoretical TiN bulk density of 5.4 g/cm^3. This high density suggests that these TiN films will be resistant to oxidation. This oxidation resistance has been confirmed by depth profile XPS measurements where there is minimal O diffusion into the TiN films. This behavior is in contrast to thermal TiN ALD films that display high porosity leading to facile oxidation.[15]

3.3. Mechanism for TiN EE-ALD with NH_3 RBG. The TiN EE-ALD films grown with the NH_3 RBG at <70 °C have high purity, high density, and crystallinity. The NH_3 RBG is facilitating the growth of these films. An illustration of TiN EE-ALD using TDMAT and low energy electrons in the presence of a continuous NH_3 RBG is shown in Figure 10. The electrons are believed to play a key role by dissociating NH_3 in the gas phase to produce $\bullet NH_2$ and $\bullet H$ radicals. These radicals can adsorb onto empty sites on the TiN surface. In addition, these radicals can abstract dimethylamine ligands from TDMAT adsorption products on the surface.

In addition to dissociating NH_3 in the gas phase, the electrons can also desorb H from $-NH_2$ species on the surface. This H ESD produces additional empty sites on the TiN surface. The TDMAT precursor can then adsorb onto these empty sites to add more Ti to the TiN surface. The electrons may also crack dimethylamine ligands on the surface and produce carbon fragments. However, the continuous flux of $\bullet NH_2$ and $\bullet H$ radicals from NH_3 dissociation may be able to remove this surface carbon as CH_3NH_2 or CH_4. The $\bullet H$ radicals may also provide a pathway for the removal of oxygen impurities as H_2O.

The primary motivation for introducing the NH_3 RBG was to ensure the complete nitridation of the TiN film. The effect of the NH_3 RBG on the film purity was an unexpected bonus that is attributed to the cleaning effect of the $\bullet NH_2$ and $\bullet H$ radicals. In addition, the possibility of introducing various RBGs offers a new parameter to tune the composition of EE-ALD films. Different films could be deposited from a single metal precursor, such as TDMAT, by changing the RBG. For example, the dissociation or adsorption of NH_3, Si_2H_6, CH_4, or B_2H_6 RBGs should form nitrides, silicides, carbides, or borides, respectively, with the metal precursor. The single RBG could also be extended to two or three RBGs to deposit ternary or quaternary EE-ALD films.

3.4. Resistivity of TiN EE-ALD Films. The resistivity of the TiN EE-ALD films was characterized using in situ four-wavelength ellipsometry and ex situ spectroscopic ellipsometry. To confirm that the TiN EE-ALD films were comparable with other TiN films, Figure 11 displays the results for the imaginary part of the pseudo dielectric function (ε_2) for the TiN EE-ALD films, TiN plasma-enhanced ALD (PE-ALD) films reported in the literature by Langereis et al.,[36] and TiN films reported in the J.A. Woollam CompleteEASE database. The results shown for the TiN EE-ALD film were obtained using ex situ spectroscopic ellipsometry.

Figure 11 shows that there is excellent agreement between these three data sets. This good correlation includes the ε_2 results at low energy where the Drude term in the ellipsometry model is related to the film resistivity. The good agreement between the ellipsometry model employed in this work and the available literature models suggests both that the model used in this work is accurate and the TiN EE-ALD film is high-quality TiN.

https://doi.org/10.1021/acs.chemmater.2c02341
Chem. Mater. 2022, 34, 9624−9633

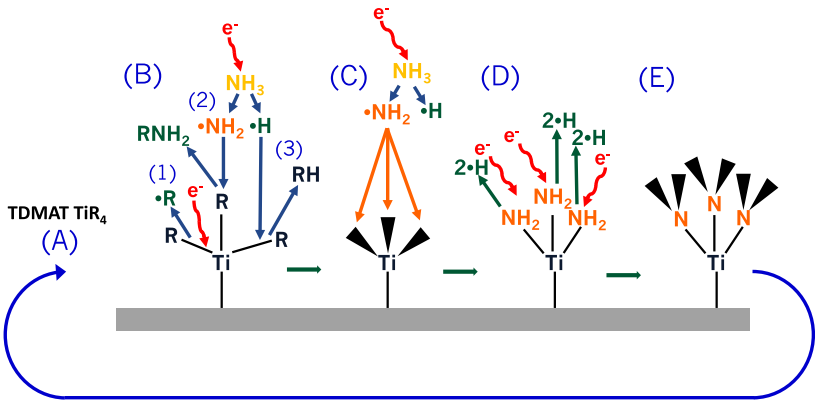

Figure 10. Mechanism for TiN EE-ALD showing (A) adsorption of the TDMAT (TiR_4) precursor; (B) removal of −R ligands by (1) ESD, (2) $\bullet NH_2$ radicals, and (3) •H radicals; (C) passivation of Ti dangling bonds by $\bullet NH_2$; (D) removal of −H by ESD (shown) or radical abstraction processes (not shown); and (E) activated TiN surface for precursor adsorption.

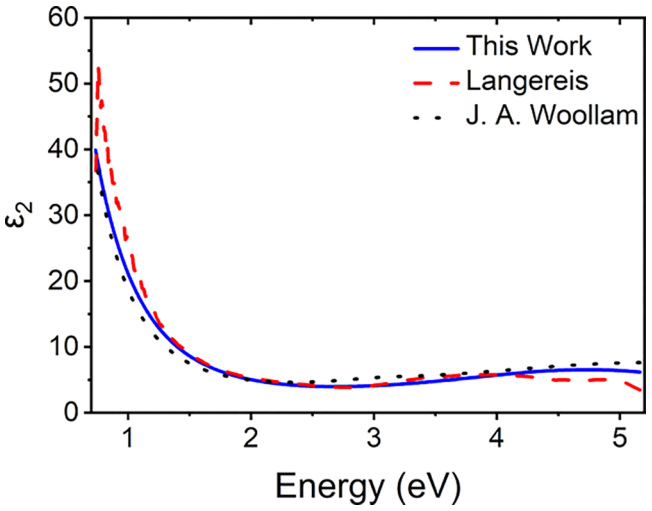

Figure 11. Comparison of experimentally measured imaginary part of the pseudo dielectric function (ε_2) between the TiN EE-ALD film on SiO_2 thermal oxide (this work) and PE-ALD TiN film (ref 36) and results for TiN in J.A. Woollam database. For the TiN EE-ALD film on SiO_2 thermal oxide, pulsing sequence in seconds was (1, 2, 20, 1) with a NH_3 background pressure of ∼1 mTorr.

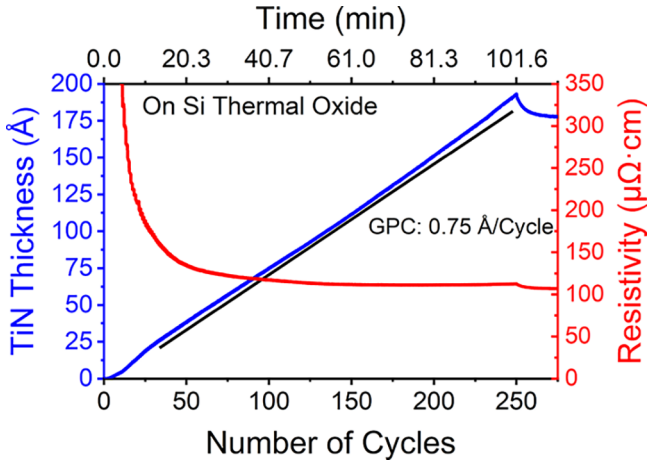

Figure 12. TiN EE-ALD film thickness and resistivity on Si thermal oxide vs number of EE-ALD cycles measured using in situ ellipsometry. Pulsing sequence in seconds was (1, 2, 20, 1) with a NH_3 background pressure of ∼1 mTorr. GPC was 0.75 Å/cycle. Resistivity reaches a value of ∼110 μΩ cm after >100 EE-ALD cycles at TiN EE-ALD film thickness of >60 Å.

The in situ ellipsometry results for the thickness and resistivity of a TiN EE-ALD film are displayed in Figure 12. These results are for TiN EE-ALD on a Si thermal oxide with a thickness of 400 nm. The dosing sequence was (1, 2, 20, 1) with a TDMAT pressure of 0.3 Torr behind the micropulse valve. Similar to the earlier results in Figures 2−5, there is rapid nucleation of the TiN EE-ALD film. The TiN film then grows linearly with a GPC of 0.75 Å/cycle over 250 EE-ALD cycles. Figure 12 also shows the corresponding resistivity of the TiN film determined from the Drude term in the ellipsometry model.

The film resistivity drops rapidly in the nucleation regime during the first 12−13 cycles. These resistivities are artificially low for film thicknesses <4 nm resulting from the inability of ellipsometry to fully account for electron scattering at grain boundaries and interfaces.[37] The film resistivity continues to decrease progressively and reaches a resistivity of ∼130 μΩ cm after 50 cycles at a film thickness of ∼40 Å. The resistivity continues to decrease slowly as the film thickness increases to ∼185 Å, where the resistivity is ∼110 μΩ cm after 250 cycles.

The EE-ALD is stopped after 250 cycles. Without the electron current impinging on the sample, the film begins to cool slightly from ∼65 °C over the next ∼10 min. This cooling results in an apparent decrease in the model film thickness of ∼16 Å and a corresponding decrease in resistivity to 104 μΩ cm. The apparent decrease in the model film thickness is associated with the temperature change of the film. The electronic properties change with temperature. The ellipsometry model interprets this temperature change as a change in film thickness.

The TiN EE-ALD film after 250 cycles in Figure 12 was also characterized by ex situ spectroscopic ellipsometry. The thickness for this film was calculated to be 173 Å from a 9 point map over a 1.5 cm × 1.5 cm area of the sample. This thickness is in good agreement with the thickness of 169 Å determined by the in situ ellipsometry after the sample cooled following the electron exposure. The Drude−Lorentz model used for the ex situ spectroscopic ellipsometry over the same nine points gave a resistivity of 125 μΩ cm. This resistivity is in good agreement with the resistivity of 104 μΩ cm determined by the in situ ellipsometry. The slightly higher resistivity from

https://doi.org/10.1021/acs.chemmater.2c02341
Chem. Mater. 2022, 34, 9624−9633

ex situ spectroscopic ellipsometry may result from some TiN film oxidation after air exposure.

Four-point probe measurements were also employed to corroborate the resistivity measurements from ellipsometry. A geometric correction factor of 0.92 was applied to the raw resistivity data to account for the small coupon size. A resistivity of 131 $\mu\Omega$ cm was obtained from 10 locations at the center of substrate immediately after the removal of the sample from the deposition chamber. This resistivity is also in good agreement with the resistivity from the ellipsometry measurements. There was a negligible increase in resistivity from the four-point probe measurement over a 24 h period after removing the film from vacuum. No increase in resistivity after prolonged air exposure suggests a dense TiN film that is resistant to oxidation.

Additional experiments were conducted on a 400 nm Si thermal oxide with 150 and 200 TiN EE-ALD cycles. These experiments were performed using the same reaction conditions as employed for the 250 TiN EE-ALD cycles shown in Figure 12. The results from the in situ ellipsometry, ex situ spectroscopic ellipsometry and four-point probe measurements are given in Table 1. There is good agreement between all the resistivity values indicating that the in situ ellipsometry results shown in Figure 12 are reliable.

Table 1. TiN EE-ALD Film Thickness and Resistivity for TiN EE-ALD Films Grown Using 150, 200, and 250 EE-ALD Cycles[a]

number of cycles	thickness (Å)	4 PP resistivity ($\mu\Omega$ cm)	ex situ ellipsometry resistivity ($\mu\Omega$ cm)	in situ ellipsometry resistivity ($\mu\Omega$ cm)
150	82	148 ± 14	130	118
200	132	135 ± 39	119	110
250	173	131 ± 8	125	105

[a]TiN EE-ALD films were grown on SiO_2 thermal oxide using a pulsing sequence in seconds of (1, 2, 20, 1) with NH_3 background pressure of ~1 mTorr. Resistivity was obtained using four-point probe techniques and ex situ and in situ ellipsometry measurements.

The TiN EE-ALD film deposits on insulating as well as on conducting samples. Electron currents on an insulating substrate might be expected to charge the substrate negatively. This negative charge would then repel additional electron current. However, if the secondary electron yield is greater than unity, then the sample would charge positive. This positive charge could then pull back secondary electrons to maintain charge neutrality. Secondary electron yields greater than unity have been measured for SiO_2 and Si_3N_4 for primary electron energies from ~100−1000 eV.[38,39] A wide range of insulating materials, such as Al_2O_3, also have secondary electron yields greater than unity.[40−42] These high secondary electron yields should allow EE-ALD to be performed on insulating substrates.

4. CONCLUSIONS

TiN EE-ALD was performed using sequential exposures of TDMAT and low energy electrons with a continuous NH_3 RBG. The TiN EE-ALD was conducted utilizing a HC-PES that can deliver a high electron flux into background gases at pressures up to several mTorr. TiN EE-ALD films were grown at temperatures of 30−70 °C using electron energies of ≤100 eV and a NH_3 RBG pressure of ~1 mTorr. Electron scattering in the background gas is not a problem until higher pressures of >5 mTorr.

Rapid nucleation of the TiN EE-ALD films was achieved on a variety of substrates including a native oxide on silicon, a SiO_2 thermal oxide and an in situ deposited silicon nitride film. GPC values of 0.75 to 1.8 Å per cycle were measured using in situ four-wavelength ellipsometry for different precursor exposures. TiN EE-ALD was accomplished on insulating substrates such as a SiO_2 thermal oxide with a thickness of 400 nm. The TiN EE-ALD is thought to be achievable on insulating substrates because the secondary electron yield at electron energies of ~100 eV is greater than unity.

The TiN EE-ALD films were high purity and slightly nitrogen-rich as demonstrated by in situ AES studies and ex situ XPS measurements. Low resistivities of ~120 $\mu\Omega$ cm for the TiN films with thicknesses of ≥60 Å were measured using in situ ellipsometry analysis. Ex situ four-point probe measurements and spectroscopic ellipsometry confirmed these low resistivities. The TiN films were crystalline as determined by XRD investigations. XRR studies also revealed that the thin TiN films had densities similar to bulk TiN films.

The high quality of the TiN EE-ALD films was attributed to the presence of the NH_3 RBG. The low energy electrons and the NH_3 RBG are believed to interact to form $\bullet NH_2$ and $\bullet H$ radical species. These radical species can react with the growing surface during TiN EE-ALD and improve the film purity. The reactive $\bullet NH_2$ and $\bullet H$ species, together with the incident electron flux leading to ESD, facilitate the low temperature growth and high purity of the TiN EE-ALD films. Many other RBGs will be able to extend the possibilities for tuning film composition and properties during EE-ALD.

AUTHOR INFORMATION

Corresponding Author

Steven M. George − *Department of Chemistry, University of Colorado, Boulder, Colorado 80309-0215, United States;* orcid.org/0000-0003-0253-9184; Email: Steven.George@colorado.edu

Author

Zachary C. Sobell − *Department of Chemistry, University of Colorado, Boulder, Colorado 80309-0215, United States*

Complete contact information is available at: https://pubs.acs.org/10.1021/acs.chemmater.2c02341

Notes

The authors declare no competing financial interest.

ACKNOWLEDGMENTS

This work was supported by the Joint University Microelectronics Program (JUMP) funded by the Semiconductor Research Corporation (SRC). The authors thank Blaine Johs from Film Sense and Marcel Junige for fruitful discussions regarding ellipsometric modeling. The authors also thank Andrew Cavanagh for performing XPS analysis. The authors would like to acknowledge Kenneth Smith and Don David from the University of Colorado Integrated Instrument Development Facility for their construction and maintenance of the HC-PES and computer interfacing.

REFERENCES

(1) Sobell, Z. C.; Cavanagh, A. S.; Boris, D. R.; Walton, S. G.; George, S. M. Hollow Cathode Plasma Electron Source for Low

Temperature Deposition of Cobalt Films by Electron-Enhanced Atomic Layer Deposition. *J. Vac. Sci. Technol., A* **2021**, *39*, 042403.
(2) Sobell, Z. C.; Cavanagh, A. S.; George, S. M. Growth of Cobalt Films at Room Temperature Using Sequential Exposures of Cobalt Tricarbonyl Nitrosyl and Low Energy Electrons. *J. Vac. Sci. Technol., A* **2019**, *37*, 060906.
(3) Sprenger, J. K.; Cavanagh, A. S.; Sun, H.; Wahl, K. J.; Roshko, A.; George, S. M. Electron Enhanced Growth of Crystalline Gallium Nitride Thin Films at Room Temperature and 100 °C Using Sequential Surface Reactions. *Chem. Mater.* **2016**, *28*, 5282−5294.
(4) Sprenger, J. K.; Sun, H.; Cavanagh, A. S.; George, S. M. Electron-Enhanced Atomic Layer Deposition of Silicon Thin Films at Room Temperature. *J. Vac. Sci. Technol., A* **2017**, *36*, 01A118.
(5) Sprenger, J. K.; Sun, H.; Cavanagh, A. S.; Roshko, A.; Blanchard, P. T.; George, S. M. Electron-Enhanced Atomic Layer Deposition of Boron Nitride Thin Films at Room Temperature and 100 °C. *J. Phys. Chem. C* **2018**, *122*, 9455−9464.
(6) Uhm, J.; Jeon, H. TiN Diffusion Barrier Grown by Atomic Layer Deposition Method for Cu Metallization. *Jpn. J. Appl. Phys., Part 1* **2001**, *40*, 4657−4660.
(7) Rha, S. K.; Lee, W. J.; Lee, S. Y.; Hwang, Y. S.; Lee, Y. J.; Kim, D. I.; Kim, D. W.; Chun, S. S.; Park, C. O. Improved TiN Film as a Diffusion Barrier Between Copper and Silicon. *Thin Solid Films* **1998**, *320*, 134−140.
(8) Wang, S. Q.; Raaijmakers, I.; Burrow, B. J.; Suthar, S.; Redkar, S.; Kim, K. B. Reactively Sputtered TiN as a Diffusion Barrier between Cu and Si. *J. Appl. Phys.* **1990**, *68*, 5176−5187.
(9) Weber, E. R. Transition Metals in Silicon. *Appl. Phys. A* **1983**, *30*, 1−22.
(10) McBrayer, J. D.; Swanson, R. M.; Sigmon, T. W. Diffusion of Metals in Silicon Dioxide. *J. Electrochem. Soc.* **1986**, *133*, 1242−1246.
(11) Gall, D. Electron Mean Free Path in Elemental Metals. *J. Appl. Phys.* **2016**, *119*, 085101.
(12) Gall, D. The Search for the Most Conductive Metal for Narrow Interconnect Lines. *J. Appl. Phys.* **2020**, *127*, 050901.
(13) Paranjpe, A.; IslamRaja, M. Chemical Vapor Deposition TiN Process for Contact/Via Barrier Applications. *J. Vac. Sci. Technol., B: Microelectron. Nanometer Struct.* **1995**, *13*, 2105−2114.
(14) Zhao, C.; Xiang, J. Atomic Layer Deposition (ALD) of Metal Gates for CMOS. *Appl. Sci.* **2019**, *9*, 2388.
(15) Elam, J. W.; Schuisky, M.; Ferguson, J. D.; George, S. M. Surface Chemistry and Film Growth during TiN Atomic Layer Deposition Using TDMAT and NH_3. *Thin Solid Films* **2003**, *436*, 145−156.
(16) Elers, K. E.; Saanila, V.; Soininen, P. J.; Li, W. M.; Kostamo, J. T.; Haukka, S.; Juhanoja, J.; Besling, W. F. A. Diffusion Barrier Deposition on a Copper Surface by Atomic Layer Deposition. *Chem. Vap. Deposition* **2002**, *8*, 149−153.
(17) Musschoot, J.; Xie, Q.; Deduytsche, D.; Van den Berghe, S.; Van Meirhaeghe, R. L.; Detavernier, C. Atomic Layer Deposition of Titanium Nitride from TDMAT Precursor. *Microelectron. Eng.* **2009**, *86*, 72−77.
(18) Tiznado, H.; Zaera, F. Surface Chemistry in the Atomic Layer Deposition of TiN Films from $TiCl_4$ and Ammonia. *J. Phys. Chem. B* **2006**, *110*, 13491−13498.
(19) Wolf, S.; Breeden, M.; Kwak, I.; Park, J. H.; Kavrik, M.; Naik, M.; Alvarez, D.; Spiegelman, J.; Kummel, A. C. Low Temperature Thermal ALD TaN_x and TiN_x Films from Anhydrous N_2H_4. *Appl. Surf. Sci.* **2018**, *462*, 1029−1035.
(20) Wang, L.; Liu, B.; Song, Z.; Feng, S.; Zhou, Z.; Xiang, Y.; Zhang, F. Atomic Vapor Deposition of TiN with Diluted Tetrakis (diethylamido) Titanium (TDEAT) for Phase Change Memory. *ECS Trans.* **2009**, *22*, 167−173.
(21) Chen, Z. X.; Li, X.; Li, W. M.; Lo, G. Q. Plasma-Enhanced Atomic Layer Deposition (PEALD) of TiN using the Organic Precursor Tetrakis(ethylmethylamido)Titanium (TEMAT). *MATEC Web Conf.* **2016**, *39*, 01010.
(22) Profijt, H. B.; Potts, S. E.; van de Sanden, M. C. M.; Kessels, W. M. M. Plasma-Assisted Atomic Layer Deposition: Basics, Opportunities, and Challenges. *J. Vac. Sci. Technol., A* **2011**, *29*, 050801.
(23) Anz, S. J.; Margolese, D. I.; Sando, S. F.; Gillis, H. P.; Goddard, W. A. Damage-Free Atomic-Scale Etching and Surface Enhancements by Electron-Enhanced Reactions: Results and Simulations. *Springer Ser. Mater. Sci.* **2021**, *284*, 603−627.
(24) Perentes, A.; Hoffmann, P. Focused Electron Beam Induced Deposition of Si-based Materials from SiO_xC_y to Stoichiometric SiO_2: Chemical Compositions, Chemical-Etch Rates, and Deep Ultraviolet Optical Transmissions. *Chem. Vap. Deposition* **2007**, *13*, 176−184.
(25) Rohdenburg, M.; Fröch, J. E.; Martinović, P.; Lobo, C. J.; Swiderek, P. Combined Ammonia and Electron Processing of a Carbon-Rich Ruthenium Nanomaterial Fabricated by Electron-Induced Deposition. *Micromachines* **2020**, *11*, 769.
(26) Shawrav, M. M.; Taus, P.; Wanzenboeck, H. D.; Schinnerl, M.; Stöger-Pollach, M.; Schwarz, S.; Steiger-Thirsfeld, A.; Bertagnolli, E. Highly Conductive and Pure Gold Nanostructures Grown by Electron Beam Induced Deposition. *Sci. Rep.* **2016**, *6*, 34003.
(27) Itikawa, Y. Cross Sections for Electron Collisions with Ammonia. *J. Phys. Chem. Ref. Data* **2017**, *46*, 043103.
(28) Raju, G. G. Electron-Atom Collision Cross Sections in Argon: An Analysis and Comments. *IEEE Trans. Dielectr. Electr. Insul.* **2004**, *11*, 649−673.
(29) Tiwald, T. E.; Thompson, D. W.; Woollam, J. A.; Paulson, W.; Hance, R. Application of IR Variable Angle Spectroscopic Ellipsometry to the Determination of Free Carrier Concentration Depth Profiles. *Thin Solid Films* **1998**, *313−314*, 661−666.
(30) Okada, L. A.; George, S. M. Adsorption and Desorption Kinetics of Tetrakis(dimethylamino)titanium and Dimethylamine on TiN Surfaces. *Appl. Surf. Sci.* **1999**, *137*, 113−124.
(31) Walz, M. M.; Schirmer, M.; Vollnhals, F.; Lukasczyk, T.; Steinrück, H. P.; Marbach, H. Electrons as "Invisible Ink": Fabrication of Nanostructures by Local Electron Beam Induced Activation of SiO_x. *Angew. Chem., Int. Ed.* **2010**, *49*, 4669−4673.
(32) Muthukumar, K.; Jeschke, H. O.; Valentí, R.; Begun, E.; Schwenk, J.; Porrati, F.; Huth, M. Spontaneous Dissociation of $Co_2(CO)_8$ and Autocatalytic Growth of Co on SiO_2: A Combined Experimental and Theoretical Investigation. *Beilstein J. Nanotechnol.* **2012**, *3*, 546−555.
(33) Vollnhals, F.; Drost, M.; Tu, F.; Carrasco, E.; Späth, A.; Fink, R. H.; Steinrück, H. P.; Marbach, H. Electron-Beam Induced Deposition and Autocatalytic Decomposition of $Co(CO)_3NO$. *Beilstein J. Nanotechnol.* **2014**, *5*, 1175−1185.
(34) Jain, A.; Ong, S. P.; Hautier, G.; Chen, W.; Richards, W. D.; Dacek, S.; Cholia, S.; Gunter, D.; Skinner, D.; Ceder, G.; Persson, K. A.; et al. Commentary: The Materials Project: A materials genome approach to accelerating materials innovation. *APL Mater.* **2013**, *1*, 011002.
(35) Behera, A. K.; Viswanath, R. N.; Lakshmanan, C.; Polaki, S. R.; Sarguna, R. M.; Mathews, T. Thermal Oxidation and Nitridation of Si Nanowalls Prepared by Metal Assisted Chemical Etching. *AIP Conf. Proc.* **2018**, *1942*, 050062.
(36) Langereis, E.; Heil, S. B. S.; van de Sanden, M. C. M.; Kessels, W. M. M. In situ Spectroscopic Ellipsometry Study on the Growth of Ultrathin TiN Films by Plasma-Assisted Atomic Layer Deposition. *J. Appl. Phys.* **2006**, *100*, 023534.
(37) Van Bui, H.; Kovalgin, A. Y.; Wolters, R. A. M. On the Difference Between Optically and Electrically Determined Resistivity of Ultra-Thin Titanium Nitride Films. *Appl. Surf. Sci.* **2013**, *269*, 45−49.
(38) Dionne, G. F. Origin of Secondary Electron Emission Yield Curve Parameters. *J. Appl. Phys.* **1975**, *46*, 3347−3351.
(39) Fijol, J. J.; Then, A. M.; Tasker, G. W.; Soave, R. J. Secondary Electron Yield of SiO_2 and Si_3N_4 Thin Films for Continuous Dynode Electron Multipliers. *Appl. Surf. Sci.* **1991**, *48−49*, 464−471.
(40) Insepov, Z.; Ivanov, V.; Jokela, S. J.; Veryovkin, I.; Zinovev, A.; Frisch, H. Comparison of Secondary Electron Emission Simulation to

https://doi.org/10.1021/acs.chemmater.2c02341
Chem. Mater. 2022, 34, 9624−9633

Experiment. *Nucl. Instrum. Methods Phys. Res., Sect. A* **2011**, *639*, 155−157.
(41) Seiler, H. Secondary Electron Emission in the Scanning Electron Microscope. *J. Appl. Phys.* **1983**, *54*, R1−R18.
(42) Tao, S. X.; Chan, H. W.; van der Graaf, H. Secondary Electron Emission Materials for Transmission Dynodes in Novel Photomultipliers: A Review. *Materials* **2016**, *9*, 1017.

Recommended by ACS

Growth Mechanism and Film Properties of Atomic-Layer-Deposited Titanium Oxysulfide
Jeroen G. A. van Kasteren, Bart Macco, *et al.*
AUGUST 22, 2022
CHEMISTRY OF MATERIALS
READ

Strong (110) Texturing and Heteroepitaxial Growth of Thin Mo Films on MoS_2 Monolayer
Jun-young Kim, Dongzhi Chi, *et al.*
OCTOBER 06, 2022
ACS APPLIED ELECTRONIC MATERIALS
READ

Oxidation-Resistant Amorphous Zinc Tin Nitride Films with Tunable Optical and Electrical Properties
Ji Woon Choi, Byungha Shin, *et al.*
JULY 19, 2022
CHEMISTRY OF MATERIALS
READ

Structural, Optical, and Electrical Properties of InO_x Thin Films Deposited by Plasma-Enhanced Atomic Layer Deposition for Flexible Device Applications
TaeHyun Hong, Jin-Seong Park, *et al.*
MAY 27, 2022
ACS APPLIED ELECTRONIC MATERIALS
READ

Get More Suggestions >

https://doi.org/10.1021/acs.chemmater.2c02341
Chem. Mater. 2022, 34, 9624−9633